J. Fluid Mech. (1993), *vol.* 257, *pp.* 575–596

The motion of an elliptical cylinder in channel flow at low Reynolds numbers

By MASAKO SUGIHARA-SEKI
National Cardiovascular Center Research Institute, Suita, Osaka 565, Japan

(Received 18 May 1992 and in revised form 29 June 1993)

The motion of an elliptical cylindrical particle immersed in an incompressible Newtonian fluid in a narrow channel is examined numerically in the zero-Reynolds-number limit. It is assumed that no external forces or torques act on the elliptical cylinder, and the effects of inertia forces on the motion of the fluid and the particle are neglected. The Stokes equations are solved by a finite-element method for various positions and orientations of the cylinder, yielding the instantaneous velocities of the particle that satisfy the conditions of zero force and zero torque on the particle. Using the computed longitudinal, lateral, and angular velocities of the particle, the evolution of the particle's position and orientation is determined for various initial configurations. An elliptical cylinder is found to either tumble or oscillate in rotation, depending on the particle-channel size ratio, the axis ratio of the elliptical cylinder, and the initial conditions. In the first case, the particle rotates continuously in one direction that is well approximated by Jeffery's solution for an elliptical cylinder in unbounded shear flow with a so-called equivalent axis ratio; in the second case, the particle changes its direction of rotation during part of each period. In both cases, the particle translates with a periodically varying longitudinal velocity, accompanied by a considerable side drift due to the walls. The oscillatory motion is more likely to occur when the particle-channel size ratio or axis ratio is increased. The tumbling motion is inhibited for elliptic cylinders whose size ratios are larger than threshold values that depend on the axis ratio.

1. Introduction

The study of the creeping motion of a neutrally buoyant particle in tube or channel flow is important for understanding blood flow in the microcirculation and the rheology of suspensions in bounded domains. In bounded flows, the motion of a particle is significantly affected by the boundaries, especially when the particle is located close to the boundaries or the particle size is comparable to the tube diameter or channel width.

In the present paper, we study the motion of a single elliptical cylindrical particle freely suspended in a narrow channel flow bounded by parallel plates. We consider elliptic cylinders as the two-dimensional analogue of ellipsoids. The ellipsoid is particularly useful in the modelling of blood and particulate suspensions, since it encompasses a wide range of shapes ranging from disks to slender bodies. While spherical particles in channel flow translate steadily parallel to the walls, ellipsoids generally show a more complicated behaviour and provide much richer information relevant to suspension rheology.

The motion of a neutrally buoyant ellipsoid in an unbounded simple shear flow at low Reynolds number was studied by Jeffery (1922), and the Stokes equations were

solved exactly in an analytical form for two cases. The first case is for an ellipsoid of revolution, i.e. a spheroid: the particle motion was found to consist of a spin about the axis of symmetry and a precession of this axis about the vorticity vector of the undisturbed flow. The second case is for a general (non-axisymmetric) ellipsoid in the special case when the ellipsoid rotates about a principal axis that is permanently aligned with the undisturbed vorticity vector. The particle was shown to rotate continuously with a periodically varying angular velocity. Since this analytical result includes only the ratio of the axes in the plane of the shear flow called equivalent axis ratio, the length of the other axis, which is parallel to the vorticity vector, is not important. Thus, taking the limit as this axis tends to infinite, we find that an elliptic cylinder has the same dynamical behaviour as an ellipsoid with the same equivalent axis ratio, as long as the ellipsoid is constrained to rotate about a principal axis that is parallel to the undisturbed vorticity. Furthermore, Jeffery showed that the solution in the second case is identical to that governing the time evolution of the projection of the symmetry axis of spheroids onto the plane of the shear flow. Therefore, in the special cases when the symmetry axis lies in the plane of the shear flow, the motion of an axisymmetric ellipsoid in an unbounded simple shear flow coincides with that of an elliptic cylinder with the same equivalent axis ratio.

These classical solutions by Jeffery, as well as those by Oberbeck (1876) and Edwardes (1892) for translation and rotation of an ellipsoid, were built up using ellipsoidal harmonics. Recent developments of different approaches such as the singularity method and multipole expansions, which are more generally applicable to particulate Stokes flow and to numerical analyses, are thoroughly reviewed by Kim & Karrila (1991).

Effects of quadratic velocity profiles on the motion of an ellipsoid were studied by Chwang (1975), who considered the motion of an ellipsoid freely floating in an unbounded paraboloidal flow using the singularity method. He found that an ellipsoid rotates as if it were immersed in a linear shear flow with a shear rate equal to that of the paraboloidal flow evaluated at the centre of the particle, and translates along a straight path parallel to the main flow direction without any side drift.

Regarding the effect of a wall on the motion of an ellipsoid, some approximate analyses have been made for an axisymmetric ellipsoid in the vicinity of a plane wall in shear flow, mainly in the cases when the symmetry axis lies in the plane of the shear flow. Dąbroś (1985) calculated the angular velocity of a freely suspended ellipsoid by the singularity method, and reported that the angular velocity is reduced owing to interaction with the wall, especially when the particle is oriented parallel to the wall. Hsu (1985) and Hsu & Ganatos (1989) computed the hydrodynamic force and torque on an ellipsoid adjacent to a wall by the boundary-integral method. Hsu (1985) extended this work to study the free motion of an ellipsoid in shear flow in the vicinity of a wall. It was demonstrated that the period of rotation increases as the particle approaches the wall, and that the particle executes a periodic motion toward and away from the wall as it is continuously tumbling forward. Yang & Leal (1984) studied the motion of a slender ellipsoid near a flat fluid–fluid interface with an arbitrary orientation, based on slender-body theory, and reported an oscillatory migration of the particle perpendicular to the interface. The presence of a wall or interface has been found to reduce the rotational velocity of an ellipsoid, and to cause a transverse drift in shear flow.

Although the motion of a freely floating ellipsoid near a single wall has been well-studied, theoretical studies of the motion in a tube or channel flow have been limited. Wakiya (1957, 1959) treated the problems of an ellipsoid in a circular tube and an

elliptic cylinder in a channel by the method of reflections, but his analysis were restricted to special cases where the major or minor axis of the particle is parallel to the undisturbed flow. Numerical studies of the axisymmetric flow due to the motion of an array of spheroids at the centreline of a circular tube reveal no rotary motions, as expected from symmetry (Chen & Skalak 1970; Tözeren 1984). Recently, the present author used a finite-element method to study the motion of a doublet consisting of two rigidly connected equal-sized circular cylinders in a channel flow (Sugihara-Seki 1992). It was shown that a doublet translates with a variable longitudinal velocity and exhibits a substantial lateral migration. The period of rotation is longer than that for unbounded flow. Furthermore, some new types of oscillatory motion were found, in which the doublet rotates but changes its direction at every half-period and moves transversely in an oscillatory manner around a mean lateral position.

In this paper, we present a numerical study of the motion of a neutrally buoyant elliptical cylindrical particle freely suspended in a two-dimensional Poiseuille flow. We consider cases where the width of the channel is comparable to the particle size. The Reynolds number is assumed to be small so that the effect of inertia forces on the motion of the fluid and the particle can be neglected. The instantaneous velocities of the elliptic cylinder at arbitrary positions and orientations in the channel and the flow of the suspending fluid are solved numerically by a finite-element method. Using the computed particle velocities and rotations, the trajectories of the particle are determined for various initial lateral positions and orientations in the channel. It will be shown that, as in the case of an ellipsoid near a plane wall (Yang & Leal 1984; Hsu 1985; Dąbroś 1986), the classical tumbling motion of the elliptic cylinder is modified owing to the channel walls, and as in the case of a doublet in a channel flow (Sugihara-Seki 1992), oscillatory motion is observed.

In §2 the formulation of the problem is presented with a brief introduction of the numerical procedure and a check of numerical accuracy. In §3 numerical results are given for the motion of an elliptic cylinder in a channel flow, and discussed in comparison with the motion in unbounded flows and the doublet motion.

2. Formulation

Consider the motion of an elliptic cylinder with semi-axis a and b in an incompressible Newtonian fluid between two infinite parallel planes with half channel width d, as shown in figure 1. It is assumed that the particle is neutrally buoyant and free of external forces and torques including Brownian forces. A Cartesian coordinate system (x, y) fixed relative to the channel walls is introduced such that the channel centreline is at $y = 0$, and the centre of the elliptic cylinder is initially at $x = 0$. The position of the elliptic cylinder at any later instant is specified by its centroidal coordinate (X, Y) and the angle of inclination θ of its major axis relative to the flow direction (see figure 1).

At low Reynolds numbers, the fluid motion satisfies the creeping-flow equations:

$$\nabla p = \mu \nabla^2 \boldsymbol{u}, \tag{1}$$

$$\nabla \cdot \boldsymbol{u} = 0, \tag{2}$$

where $\boldsymbol{u}$, p and μ are respectively the velocity, the pressure, and the viscosity of the fluid.

Far upstream and downstream from the particle, the velocity distribution approaches that due to Poiseuille flow; i.e.

$$\boldsymbol{u} \to (U_{max}(1 - y^2/d^2), 0) \quad \text{as } x \to \pm\infty. \tag{3}$$

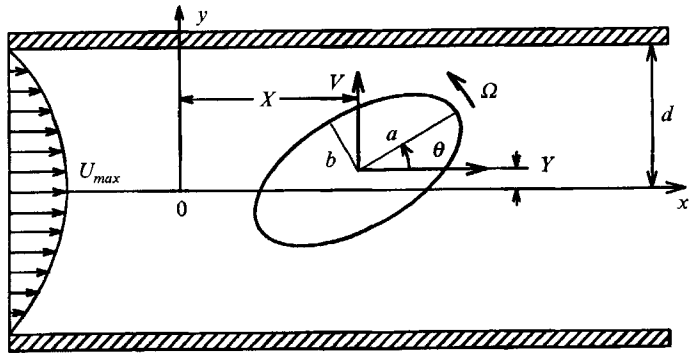

FIGURE 1. Configuration for an elliptic cylinder freely floating in a channel flow.

We require the no-slip and no-penetration boundary condition on the walls and the particle. If the centre of the cylinder translates at a velocity $\boldsymbol{U} = (U, V)$ and rotates at an angular velocity Ω, then the boundary conditions are

$$\boldsymbol{u} = \boldsymbol{0} \quad \text{at } y = \pm d, \tag{4}$$

and

$$\boldsymbol{u} = \boldsymbol{U} + \Omega \boldsymbol{k} \times \boldsymbol{r} \quad \text{at the surface of the particle,} \tag{5}$$

where $\boldsymbol{r}$ is the radial vector relative to the centre of the particle and $\boldsymbol{k}$ is the unit vector in the z-direction. The values of $\boldsymbol{U}$ and Ω are determined as part of the solution by the condition that the resultant force and torque exerted on the particle by the fluid stresses on its surface vanish.

$$\oint \boldsymbol{\sigma} \cdot \mathrm{d}\boldsymbol{s} = \boldsymbol{0}, \tag{6}$$

and

$$\oint \boldsymbol{r} \times (\boldsymbol{\sigma} \cdot \mathrm{d}\boldsymbol{s}) = \boldsymbol{0}, \tag{7}$$

where $\boldsymbol{\sigma}$ and $\mathrm{d}\boldsymbol{s}$ represent the stress tensor and a surface element of the particle, respectively, and the integrations are carried out over the surface of the particle.

In the numerical formulation, condition (3) is replaced by

$$\boldsymbol{u} = (U_{max}(1 - y^2/d^2), 0) \quad \text{at } x = X \pm l, \tag{8}$$

where l is sufficiently larger than d; in most cases, we adopted $l/d = 5$. Differences between the solutions for $l/d = 5$ and $l/d = 10$ obtained by our method are found to be less than 0.1 % for all cases examined. This suggests that $l/d = 5$ is large enough for condition (8) to be sufficiently accurate.

Given the position and orientation of the elliptic cylinder, its motion and the flow of the suspending fluid in the region D $\{(x, y): X - l \leqslant x \leqslant X + l, -d \leqslant y \leqslant d\}$ are computed by a finite-element method, based on a variational principle (Sugihara & Niimi 1984; Sugihara-Seki & Skalak 1988). A variational functional that produces the Stokes equations may be obtained as (Olson & Tuann 1978)

$$J = \int_D \left[\mu \left\{ \left(\frac{\partial u}{\partial x}\right)^2 + \left(\frac{\partial v}{\partial y}\right)^2 + \frac{1}{2}\left(\frac{\partial u}{\partial y} + \frac{\partial v}{\partial x}\right)^2 \right\} - p\left(\frac{\partial u}{\partial x} + \frac{\partial v}{\partial y}\right) \right] \mathrm{d}x\,\mathrm{d}y. \tag{9}$$

Requiring that J is stationary with respect to $(\boldsymbol{u}, p)$ and $(\boldsymbol{U}, \Omega)$ under the conditions (4),

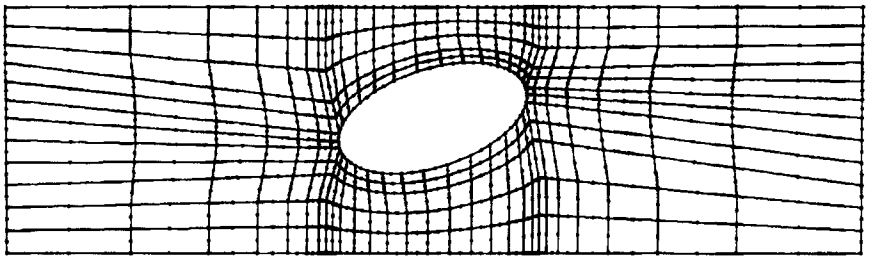

FIGURE 2. Typical grid and nodal points used in the finite-element method.

(5) and (8), yields equations (1), (2), (6) and (7) as Euler equations of the variational principle.

In the numerical procedure, D is divided into a number of finite elements. A representative grid and nodal points are shown in figure 2. Each element is a quadrilateral with four corner nodes and four side nodes. Using the values of the velocity at the eight nodes and the values of pressure at the four corner nodes, the velocity and pressure within each element are approximated by polynomial functions in terms of local coordinates. Substituting the expressions for the velocity and pressure into (9) and following a variational principle, we obtain a set of linear equations for the nodal values of $(\boldsymbol{u}, p)$, U and Ω (Sugihara-Seki & Skalak 1988). These equations are solved numerically using a Gaussian elimination method, under the boundary conditions (4), (5) and (8). In a typical numerical computation with 308 elements, 1036 nodes and 2117 unknowns, the CPU time for the computation of one configuration with double precision was less than 4 s on the FACOM VP-2600 at the Data Processing Center, Kyoto University, Japan.

The instantaneous translational velocity U and angular velocity Ω of an elliptic cylinder, as well as the nodal values of $(\boldsymbol{u}, p)$ of the fluid, were computed for a range of physically accessible values of the lateral position Y/d and angle of inclination θ, in the range of $0 \leqslant Y/d < 1$ and $0 \leqslant \theta \leqslant \frac{1}{2}\pi$, for several values of the aspect ratio $\alpha(= a/b)$ and size ratio $\beta(= ab/d^2)$. Using the instantaneous velocities of the particle, the temporal changes of X, Y and θ were calculated as follows. First, the longitudinal velocity U_0, the lateral velocity V_0, and the angular velocity Ω_0 of the particle appropriate to the current configuration (X_0, Y_0, θ_0) are obtained by a bilinear interpolation using a set of the computed velocities at neighbouring points in the (Y, θ) space. Then, the current configuration is changed to a new one in a small time-step Δt in such a way that $X' = X_0 + U_0 \Delta t$, $Y' = Y_0 + V_0 \Delta t$ and $\theta' = \theta_0 + \Omega_0 \Delta t$, where (X', Y', θ') represent the new configuration. By repeating this procedure, the transient motion of the particle is determined for arbitrary initial configurations (Sugihara-Seki & Skalak 1989; Sugihara-Seki, Secomb & Skalak 1990). A step size Δt is chosen so that the particle returns to the initial configuration after a period of motion, within an accuracy of 10^{-3} in the $(Y/d, \theta)$-space.

In order to assess the numerical accuracy of the present finite-element method, we compare our results with exact solutions or approximate solutions obtained by a method of reflections or a numerical method, in three cases of (*a*) a circular cylinder at the channel centreline in a Poiseuillle flow, (*b*) a small circular cylinder adjacent to a wall in a Couette flow, and (*c*) a small elliptic cylinder in a channel flow, with the major or minor axis parallel to the walls.

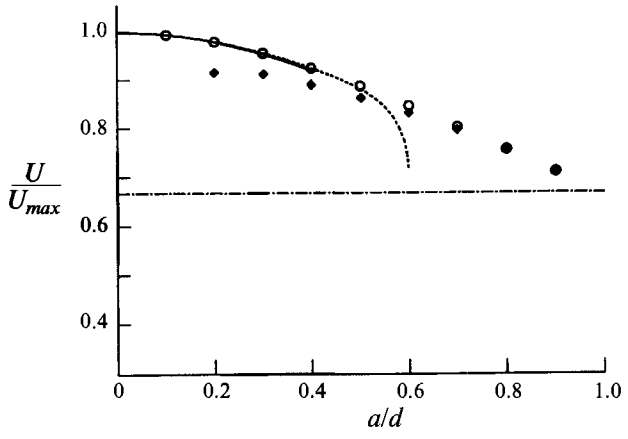

FIGURE 3. Non-dimensional longitudinal velocities of neutrally buoyant circular cylinders in a Poiseuille flow placed midway between the channel walls. ——, approximate solutions by Takaisi (1955, 1956); – – –, approximate solutions by Faxen (1946); ◆, numerical solutions by Dvinsky & Popel (1987); ○, present results.

(*a*) *A circular cylinder in channel flow*

The forces exerted on a small circular cylindrical particle located midway between the channel walls were analytically calculated by the method of reflections, when it is translating steadily along the channel in an otherwise quiescent fluid, or held fixed in a Poiseuille flow (Faxen 1946; Takaisi 1955, 1956). These two solutions are superimposed to get a translational velocity of a circular cylinder freely suspended in a Poiseuille flow. Dvinsky & Popel computed a translational velocity of a neutrally buoyant circular cylinder in a channel flow, utilizing a numerically generated boundary-conforming coordinate system (Dvinsky 1983; Dvinsky & Popel 1987). Figure 3 gives a comparison of the translational velocities obtained by these methods and the present method, for a freely floating circular cylinder located at the channel centreline. Our solutions coincide with the approximate solutions by Faxen and Takaisi, for the radius ratio $a/d(=b/d) \leqslant 0.4$. In the range of larger ratios where the approximate solutions become inapplicable, our solutions agree with the numerical results by Dvinsky & Popel (1987), which give somewhat lower values for smaller ratios. Thus, the particle velocities obtained by the present method are shown to be accurate for particle size to channel width ratio up to 0.9. For larger ratios, there is no available data with which to compare our solutions. In the present study we consider elliptic cylinders whose major axis is less than 0.95 of the channel width.

(*b*) *A circular cylinder near a wall in a Couette flow*

The motion of a circular cylinder in shear flow near a stationary plane wall can be computed exactly using bipolar coordinates. The translational and rotational velocities are given as (Darabaner, Raasch & Mason 1967):

$$U = U_0 \xi, \quad \Omega = \Omega_0 \xi, \tag{10}$$

where $\xi = (1-(a/y_0)^2)^{\frac{1}{2}}$, U_0 is the undisturbed translational velocity of the cylinder (i.e. with no wall effect), Ω_0 is the undisturbed angular velocity, and y_0 is the distance of the cylinder centre from the wall. In order to compare our result with the above exact solution, we applied the present numerical scheme to compute the motion of a small

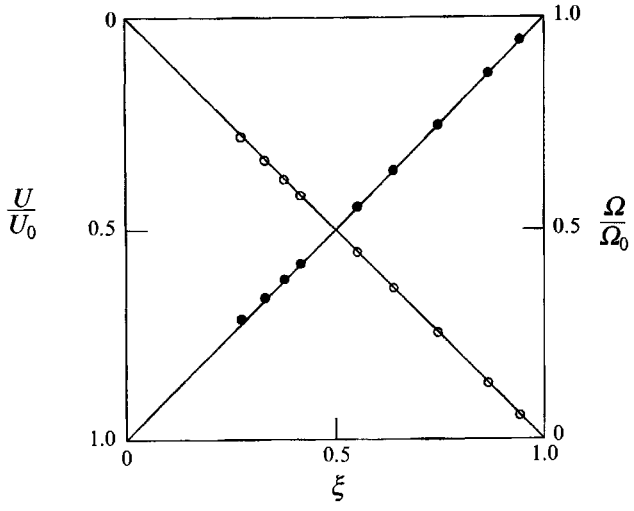

FIGURE 4. ○, the longitudinal velocity and ●, the angular velocity of a neutrally buoyant circular cylinder near a stationary wall in a Couette flow ($a/d = 0.02$). The straight lines represent exact solutions (equations (10)), for a circular cylinder in shear flow adjacent to a plane wall.

β...	0.036			0.009		
α...	2	1	0.5	2	1	0.5
Wakiya (1959)	0.991	0.981	0.965	0.998	0.995	0.991
Present results	0.9911	0.9824	0.9654	0.9978	0.9955	0.9907

TABLE 1. Non-dimensional longitudinal velocity U/U_{max} of neutrally buoyant elliptic cylinders with the semi-axis a parallel to the channel walls at the centreline in a Poiseuille flow

circular cylinder adjacent to a wall in a Couette flow, where the neighbouring wall is stationary and the distant wall translates steadily in its plane. Figure 4 shows the results for a circular cylinder with $a/d(= b/d) = 0.02$. In this case, the channel width is a hundred times the cylinder radius, so that the effect of the distant wall on the motion of the particle is considered to be small. The excellent agreement between our results and the exact solution (10) indicates that the computed particle velocities are accurate within 0.5% for gap width as small as one-tenth of the particle radius ($y_0/a = 1.1$ or $\xi = 0.417$). The error becomes approximately 1% for $y_0/a = 1.06$ ($\xi = 0.332$), and 4% for $y_0/a = 1.04$ ($\xi = 0.275$). To get more accurate results, finer meshes are required, especially in the gap region. In the present study, computations were performed only for the gap width larger than one-tenth of $(ab)^{\frac{1}{2}}$.

(*c*) *A small elliptic cylinder in channel flow*

Wakiya (1959) used the method of reflections to consider an elliptic cylinder in a channel flow, with the major or minor axis parallel to the walls. As shown in table 1, a good agreement is obtained between his solutions and the present results.

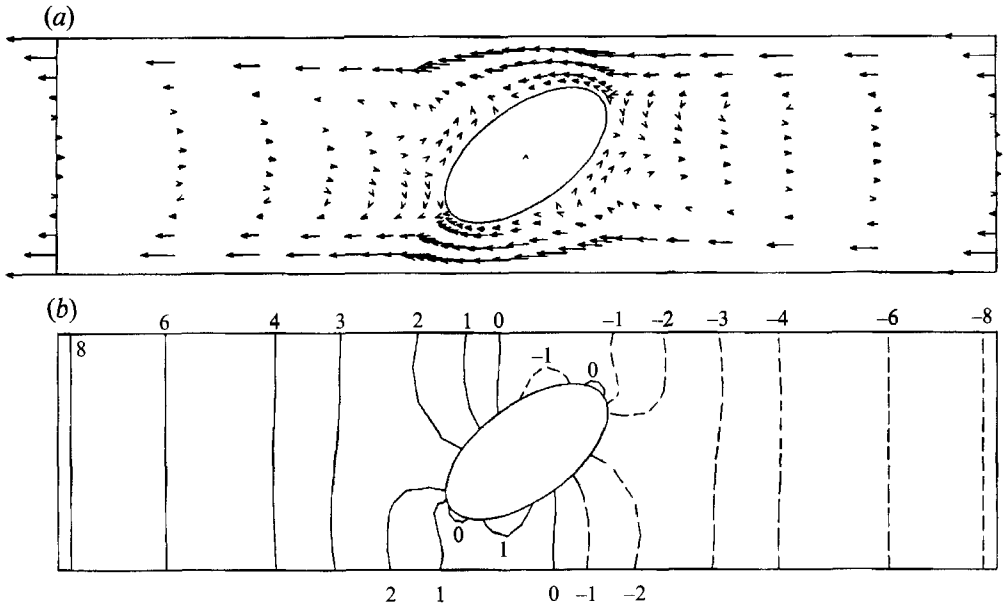

FIGURE 5. (*a*) Velocity vectors of the suspending fluid relative to the longitudinal velocity of a neutrally buoyant elliptic cylinder with $\alpha = 2$ and $\beta = 0.32$ ($a/d = 0.8$, $b/d = 0.4$), located at the channel centreline with $\theta = 0.2\pi$. The direction of the lateral motion of the cylinder is also shown by the arrow at the particle centroid. (*b*) Pressure contours around the particle. The numbers denote the values of $(p-p_m)d/\mu U_{max}$, where p_m represents the average of the upstream (at $x = X-l$) and downstream pressures (at $x = X+l$).

3. Results and discussion

3.1. *Velocity field and particle velocities*

As an example of computed results, figures 5(*a*) and 5(*b*) show velocity vectors and pressure contours in the suspending fluid for an elliptic cylinder with $\alpha = 2$ and $\beta = 0.32$ located at the centreline at an inclination angle $\theta = 0.2\pi$. In figure 5(*a*), each arrow represents the velocity vector of the fluid relative to the longitudinal velocity of the cylinder U. In this frame of reference, the walls move from right to left at velocity U. Since the cylinder is placed midway between the walls, it exhibits only a lateral motion with no rotation, as expected from symmetry and reversibility arguments. It is interesting to note the eddies upstream and downstream of the particle extending to infinity (Ganatos, Weinbaum & Pfeffer 1982). Figure 5(*b*) shows that the pressure varies considerably along the circumference of the particle, especially in the gap regions between the particle and the walls. The upward migration of the particle may be mainly attributed to the negative pressure acting on the particle in the upper gap and the positive pressure in the lower gap.

Next, we consider the velocities of cylinders at various configurations. Figure 6 shows the non-dimensional velocities U/U_{max}, V/U_{max}, $\Omega d/U_{max}$, and the additional pressure drop $\Delta(p-p_0)d/\mu U_{max}$ due to the particle, for elliptic cylinders with $\alpha = 2$ and various size ratios located at some lateral positions. Here, p_0 denotes the pressure in the absence of the cylinder (i.e. owing to the undisturbed Poiseuille flow) and Δ denotes the difference between the upstream (at $x = X-l$) and downstream values (at $x = X+l$). Generally, the curves shown in figure 6 are similar in shape for various values of $\beta(= ab/d^2)$. The longitudinal velocity of the cylinder is highest when its major axis is aligned with the direction of flow ($\theta = 0$) and lowest when it is at right angles

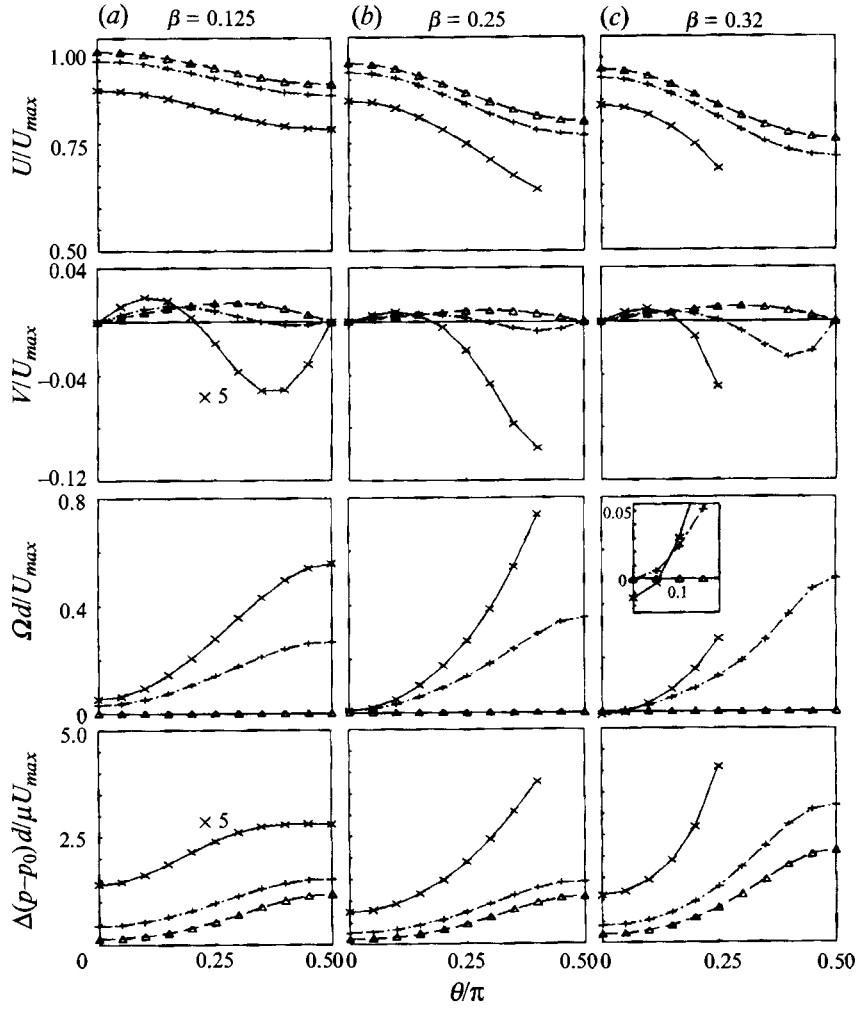

FIGURE 6. Non-dimensional velocities U/U_{max}, V/U_{max}, $\Omega d/U_{max}$, and additional pressure drop $\Delta(p-p_0)d/\mu U_{max}$, for neutrally buoyant elliptic cylinders with $\alpha = 2$ and (*a*) $\beta = 0.125$, (*b*) $\beta = 0.25$ and (*c*) $\beta = 0.32$, at lateral positions: △, $Y/d = 0$; +, $Y/d = 0.15$; ×, $Y/d = 0.3$.

($\theta = \frac{1}{2}\pi$). The lateral velocity of the cylinder at the channel centreline is positive for orientations $0 < \theta < \frac{1}{2}\pi$, and zero for $\theta = 0$ and $\frac{1}{2}\pi$. For off-centre positions, V is positive at small inclinations and negative at large inclinations. A change in the sign of the lateral velocity at a particular orientation between 0 and $\frac{1}{2}\pi$ has also been reported for an ellipsoid in shear flow adjacent to a wall (Hsu 1985).

The angular velocity vanishes when the centre of an elliptic cylinder is located at the channel centreline for all inclinations θ. For off-centre particles, Ω is minimum at $\theta = 0$ and increases with increasing θ to a maximum at $\theta = \frac{1}{2}\pi$. It is rather peculiar that the angular velocity at small inclination angles decreases with increasing β at given lateral positions, until it becomes negative for a large elliptic cylinder with $\beta = 0.32$ (see figure 6*c*). In previous studies, the rotary motion of a neutrally buoyant ellipsoid was shown to be always in the same direction as the vorticity of the undisturbed flow, in an unbounded or bounded shear flow (Jeffery 1922; Dąbroś 1985; Hsu 1985), and in unbounded paraboloidal flow (Chwang 1975). That is also true for a doublet of

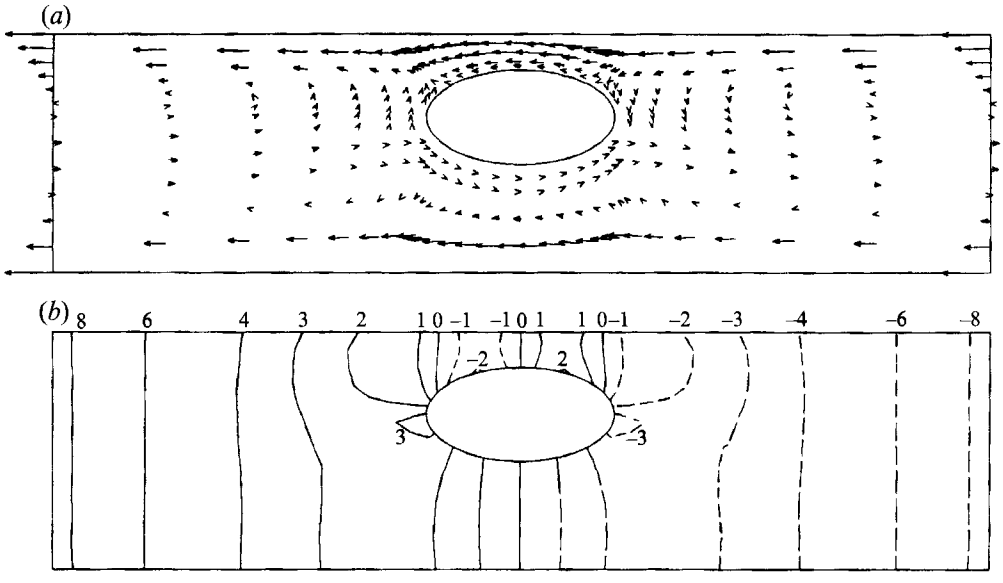

FIGURE 7. (*a*) Velocity vectors and (*b*) pressure contours around an elliptic cylinder with $\alpha = 2$ and $\beta = 0.32$, at $Y/d = 0.3$ and $\theta = 0$ (legend as in figure 5).

circular cylinders in contact in a channel flow (Sugihara-Seki 1992). Therefore, the presence of a negative angular velocity (figure 6*c*) appears as an unusual characteristic of the elliptic cylinder in channel flow. Figure 7, which shows the velocity vectors and pressure contours around an elliptic cylinder with $\alpha = 2$ and $\beta = 0.32$ at $Y/d = 0.3$ and $\theta = 0$, may provide insights to understand this phenomenon. As a particle approaches a wall or a particle becomes larger relative to the channel width, and thus the gap width between the particle and a wall is reduced, figure 7(*b*) indicates that the pressure increases in the downstream part of the gap, and decreases in the upstream part. This variation in pressure will generate a negative torque on the particle, opposing the positive torque generated by shear stresses mainly due to the Poiseuille flow. If the gap is so narrow that the negative torque due to the pressure variation is large enough, then it will tend to rotate in the negative direction, as shown in figure 6(*c*) (see also figure 8(*c*).

Another interesting feature of the rotary motion shown in figure 6 is that at $\theta = \frac{1}{2}\pi$, the angular velocity for $Y/d = 0.3$ in figure 6(*a*) is equal to approximately twice that for $Y/d = 0.15$. Since the shear rate in the Poiseuille flow is proportional to the lateral coordinate, this suggests that the ratio of the angular velocity of a small cylinder at $\theta = \frac{1}{2}\pi$ and the local shear rate of the undisturbed flow is fairly insensitive to the lateral position of the particle. This trend has been also found for an ellipsoid in shear flow near a wall (Dąbroś 1985; Hsu 1985). A further examination of the numerical results shows that, although this ratio is nearly constant in a certain range of lateral positions, it gradually increases as the particle approaches the wall up to the gap width which is approximately equal to one-tenth of $(ab)^{\frac{1}{2}}$. This is in contrast to the result that the ratio of the angular velocity at $\theta = 0$ to the local shear rate decreases with increasing the lateral position of the particle.

The additional pressure drop due to the cylinder depends strongly on the orientation of the particle, as well as on its size and lateral position. As expected, it is a minimum at $\theta = 0$ and increases with increasing θ to its maximum at $\theta = \frac{1}{2}\pi$, and the value at $\theta = \frac{1}{2}\pi$ is several times that for $\theta = 0$. The increase in the additional pressure drop with

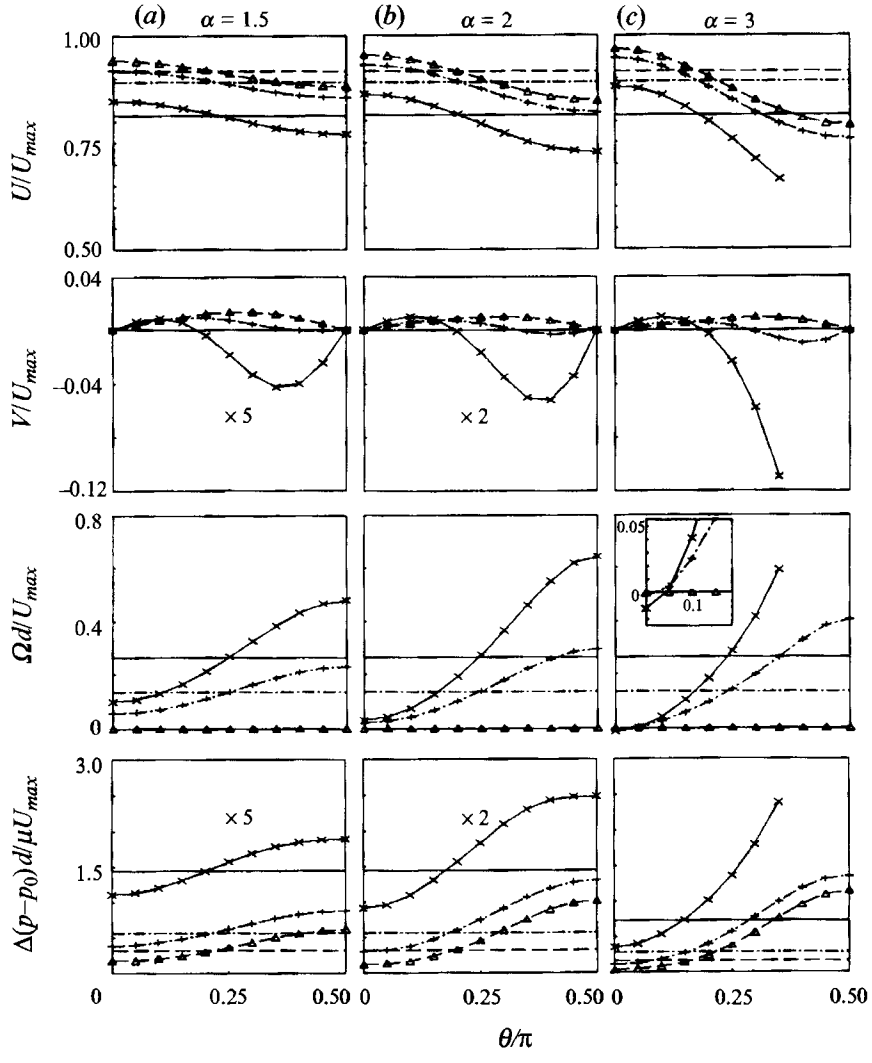

FIGURE 8. Non-dimensional velocities U/U_{max}, V/U_{max}, $\Omega d/U_{max}$, and additional pressure drop $\Delta(p-p_0)d/\mu U_{max}$, for neutrally buoyant elliptic cylinders with $\beta = 0.18$ and (*a*) $\alpha = 1.5$, (*b*) $\alpha = 2$ and (*c*) $\alpha = 3$, at lateral positions: △, $Y/d = 0$; +, $Y/d = 0.15$; ×, $Y/d = 0.3$. The values for a circular cylinder with $\alpha = 1$ and $\beta = 0.18$ are ---, for $Y/d = 0$; —·—, for $Y/d = 0.15$; ——, for $Y/d = 0.3$.

particle orientation is more significant for larger particles. It is interesting to note that the additional pressure drop computed for a given lateral position of the cylinders with various β (and/or various α) is well correlated with the minimum gap width between the particle and the channel walls. This result suggests that the increase of the additional pressure drop with particle orientation shown in figure 6 (see figure 8 also) is attributed to the decrease of the gap width with increasing θ, and that the influence of the orientation, the axis ratio, or the longitudinal length of the particle on the additional pressure drop is not large if the gap width is kept constant.

In figure 8, the variables shown in figure 6 are plotted for cylinders with size ratio $\beta = 0.18$ and various axis ratios. The variations of all variables with the inclination angle θ are similar for the different α, but they are more pronounced for slender

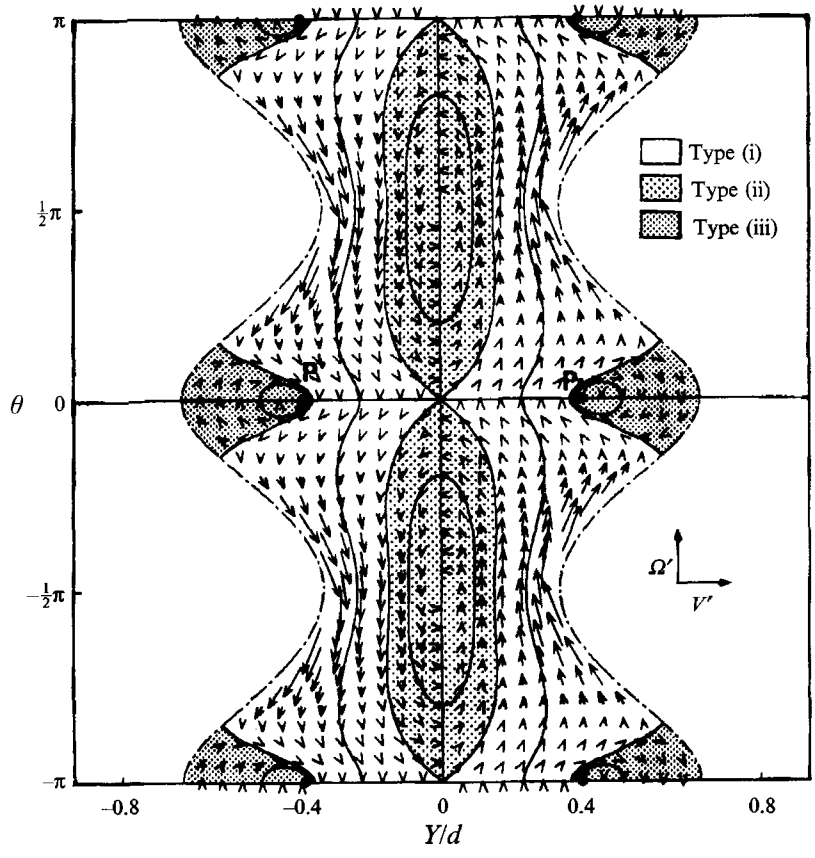

FIGURE 9. Non-dimensional lateral velocity $V' = V/U_{max}$ and angular velocity $\Omega' = \Omega d/U_{max}$ of an elliptic cylinder with $\alpha = 2$ and $\beta = 0.25$ ($a/d = 0.707$, $b/d = 0.354$). Each arrow shows a vector (V', Ω') when the lateral position and orientation of the elliptic cylinder are represented by the coordinates $(Y/d, \theta)$ at the origin of the arrow. ——, temporal variations of the lateral position and orientation of the cylinder starting from several initial values. —·—, the critical configurations at which the cylinder touches the channel walls.

particles with large α. In particular, as α increases at given Y, the angular velocity at small inclination angles decreases and becomes negative at $\alpha = 3$ (see figure 8*c*), while the angular velocity near $\theta = \frac{1}{2}\pi$ increases with the axis ratio α. It is seen that the horizontal straight lines for a circular cylinder with $\beta = 0.18$ lie between the corresponding values at $\theta = 0$ and $\frac{1}{2}\pi$ for elliptic cylinders.

3.2. *Trajectories of elliptic cylinders*

In order to analyse the trajectories of an elliptic cylinder starting from various initial configurations, vectors of $(V/U_{max}, \Omega d/U_{max})$ computed for an elliptic cylinder with $\alpha = 2$ and $\beta = 0.25$ are plotted in the $(Y/d, \theta)$ plane in figure 9. The solid curves show temporal history in lateral position and orientation of some typical cases. It appears that both V and Ω vanish at $(Y/d, \theta) = (0, (n/2)\pi)$ ($n = 0, \pm 1, \pm 2$), which means that the particle at these configurations undergoes a steady motion. The points $(Y/d, \theta) = (0, \pm\frac{1}{2}\pi)$ are neutrally stable while the points $(0, 0)$ and $(0, \pm\pi)$ represent saddle points. It is obvious from the solid curves representing the particle trajectories that all particle motions (except the steady state points) are periodic, and three types of motion of the elliptic cylinder may occur depending on its initial conditions: type

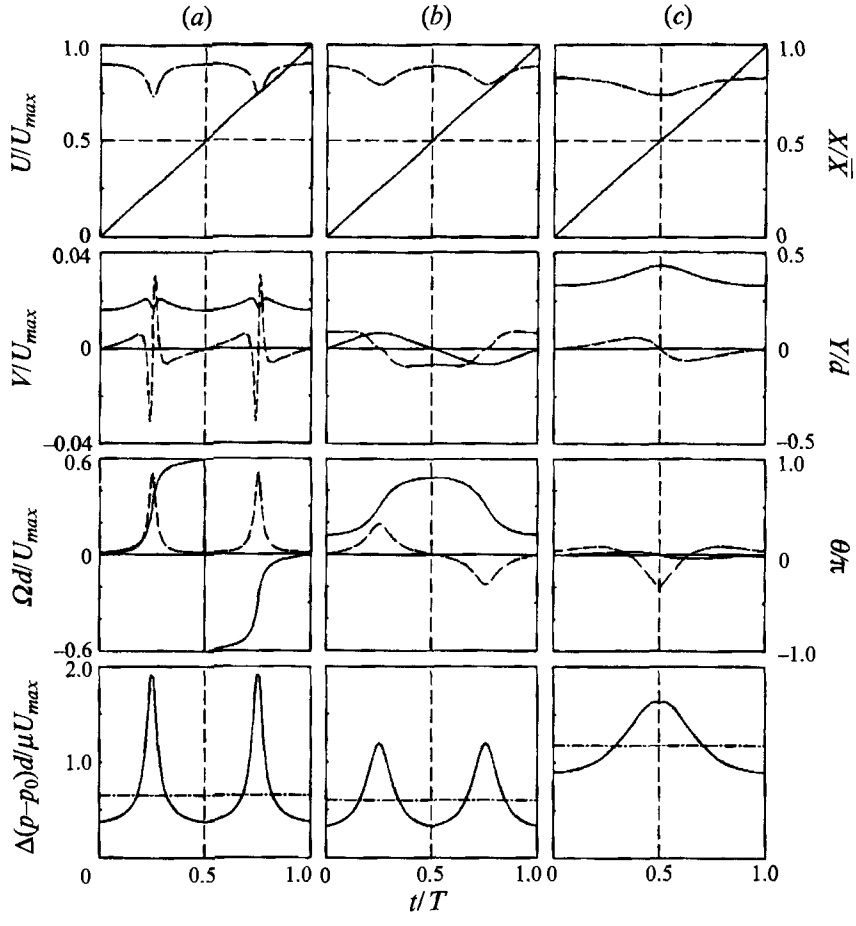

FIGURE 10. Time courses of the longitudinal and lateral positions $X/\bar{X}$, Y/d, the orientation angle θ, and the additional pressure drop $\Delta(p-p_0)\,d/\mu U_{max}$, over a complete cycle for an elliptic cylinder with $\alpha = 2$ and $\beta = 0.25$. The time courses of the velocities of the elliptic cylinder U/U_{max}, V/U_{max}, and $\Omega d/U_{max}$ are also shown by the dashed curves. (*a*) Type (i) motion starting from $(Y/d, \theta) = (0, 2, 0)$, (*b*) type (ii) motion starting from $(0, 0, 2\pi)$, and (*c*) type (iii) motion starting from $(0.33, 0)$. —·—, the temporal average of the additional pressure drop. In (*c*), the angular velocity is scaled up by 10 times, for clarity.

(i), Y/d is never zero and the particle continuously rotates in the same direction; type (ii), a particle located near the centreline rotates changing its direction as it crosses $Y/d = 0$ at every half period; type (iii), a particle far from the centreline oscillates in rotation and lateral position, with the major axis almost parallel to the channel wall.

Typical examples of evolutions of longitudinal and lateral positions and orientation $X/\bar{X}$, Y/d, θ, and the additional pressure drop $\Delta(p-p_0)\,d/\mu U_{max}$, as well as the particle velocities U/U_{max}, V/U_{max}, $\Omega d/U_{max}$, are plotted over a period as a function of time t/T in figure 10. Here, T represents a period of motion, and $\bar{X}$ denotes the longitudinal distance at which the particle advances over a period. For type (i) and type (ii) motions, the longitudinal velocity has a minimum value at $t/T = 0.25$ and 0.75 where its major axis is perpendicular to the flow, and it is almost constant for other orientations (see figure 10*a*, *b*). This longitudinal surge of the elliptic cylinder is analogous to the 'jerking' motion of an ellipsoid in unbounded paraboloidal flow, in which the ellipsoid translates with a periodically varying speed (Chwang 1975). Since in unbounded

uniform or shear flow, an ellipsoid translates at a constant velocity, the longitudinal surge is considered to be a characteristic of paraboloidal flows. The channel walls also affect the particle velocity, and the effect varies according to the particle orientation and separation from the walls. Thus, the combined effects of the Poiseuille velocity profile and the channel walls contribute to the variation in the computed longitudinal velocity.

With regard to transverse drift, the elliptic cylinder has a considerable lateral velocity for all types of motion. This is undoubtedly due to wall effects, because no side drift takes place for an ellipsoid or an elliptic cylinder in an unbounded shear flow (Jeffery 1922) or an ellipsoid in an unbounded paraboloidal flow (Chwang 1975). In particular, the lateral velocity markedly varies around $t/T = 0.25$ and 0.75 in figure 10(a), and the particle moves from one side of the channel to the other at every half period in figure 10(b).

The curves of angular velocity and orientation in the type (i) motion (figure 10a) show that the cylinder continuously rotates in one direction during a period, slowly when it is aligned with the undisturbed flow, and faster when it is aligned perpendicular to the flow. This rotary motion of an elliptic cylinder is reminiscent of its tumbling motion in unbounded shear flow, which was illustrated by Jeffery (1922). As the axis ratio α or size ratio β increases at given initial conditions, the angular velocity in the type (i) motion behaves more like a delta function with peaks situated at $t/T = 0.25$ and 0.75, an the orientation θ behaves more like a step function with step discontinuities around the stationary values, 0 and $\pm\pi$. In the type (ii) and type (iii) motions, on the other hand, the particle rotates in an oscillatory manner. For example, in figure 10(b), starting from an initial orientation, say θ', the cylinder rotates in the counter-clockwise direction within a half-period, as θ increases to a maximum orientation at $t/T = 0.5$. In the second half-period of motion, the particle rotates in the clockwise direction to return to $\theta = \theta'$ at $t/T = 1$. It is noted that the maximum angle at $t/T = 0.5$ is equal to $\pi - \theta'$, which may be derived from considerations of the flow geometry. In the type (iii) motion, the variations in orientation and angular velocity are small (note that the angular velocity in figure 10(c) is scaled up by ten times). This reflects the small oval trajectories of the type (iii) motion shown in figure 9. As a limiting case of the type (iii) motion, closed loops of the particle path in figure 9 are reduced to single points (points P and P'). At these points, both V and Ω vanish, so that the particle motion is steady.

The additional pressure drop due to the presence of an elliptic cylinder also varies significantly with time, owing to variations in the particle positions and orientations, and has sharp peaks when the cylinder is oriented perpendicular to the flow direction or placed close to the channel walls. The peaks are sharper for the type (i) motion, as the axis ratio α or the size ratio β increases at given initial conditions.

In figure 11, the Y-coordinate of the point P, Y^*, is plotted as a function of the size ratio β, or the non-dimensional length of the semi-major axis a/d. Figure 11(a) shows that Y^* decreases with increasing β, until it reaches zero at a threshold β^*, which depends on the axis ratio α. The threshold value β^* for $\alpha = 2$ is found to be approximately equal to 0.334. In figure 11(b), the three curves approach each other, suggesting that the length of the major axis has a stronger influence than the size ratio to determine the value of Y^*. The threshold values of a/d corresponding to β^* decrease with increasing α. It is of interest that Y^* at given a/d is smaller for larger α. This trend demonstrates that the region of type (iii) motion in the $(Y/d, \theta)$-plane extends closer to the origin for more slender elliptic cylinders with constant major axes (see figure 9).

On the other hand, an increase in Y^* with decreasing β or a/d for given α shown as figure 11 indicates that for small elliptic cylinders, the region of type (iii) motion in the

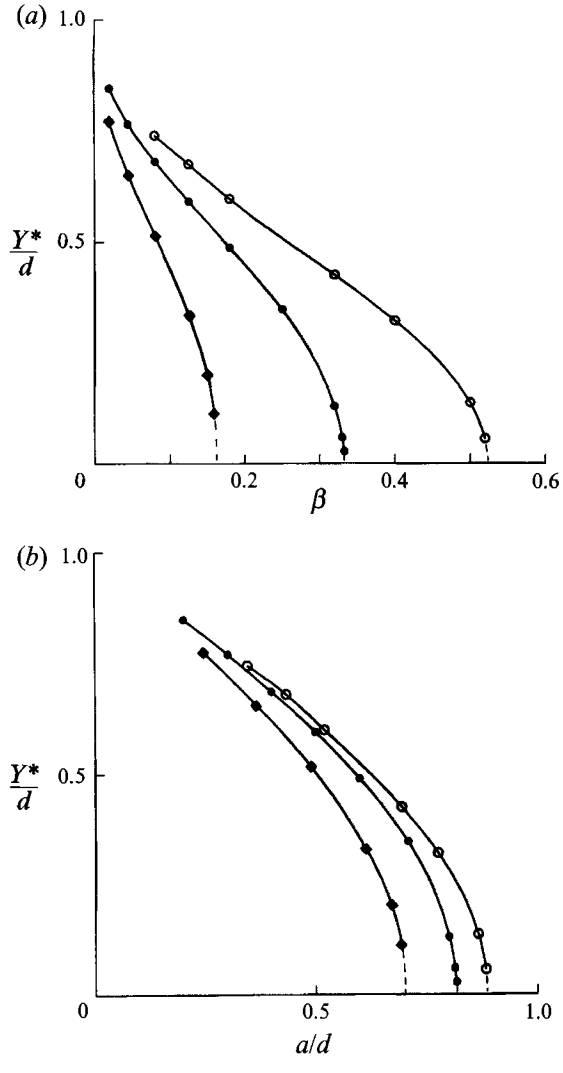

FIGURE 11. Non-dimensional lateral positions, Y^*/d, at which both of V and Ω vanish for elliptic cylinders aligned with the undisturbed flow ($\theta = 0$), with ○, $\alpha = 1.5$; ●, $\alpha = 2$; and ◆, $\alpha = 3$. (*a*) Y^*/d *vs.* β, and (*b*) Y^*/d *vs.* a/d.

$(Y/d, \theta)$-plane is restricted to two marginal regions near the Y/d-axis, just below the maximum and just above the minimum of Y/d (see figure 9). In other words, a small elliptic cylinder undergoes the type (iii) motion only when it is located in the vicinity of the channel walls, with its major axis almost parallel to the undisturbed flow. In the type (iii) motion, the cylinder has small lateral and angular velocities, and it does not change the lateral position and orientation at all if the initial configuration coincides with the points corresponding to P or P' in figure 9. Thus, the results show that small oscillatory motions of elliptic cylinders are possible when they are located close to the channel walls, with their major axes nearly aligned with the undisturbed flow. The possibility of such a nearly steady motion of elliptic cylinders is due to the presence of the walls.

In order to illustrate the motion of an elliptic cylinder with the size ratio above the

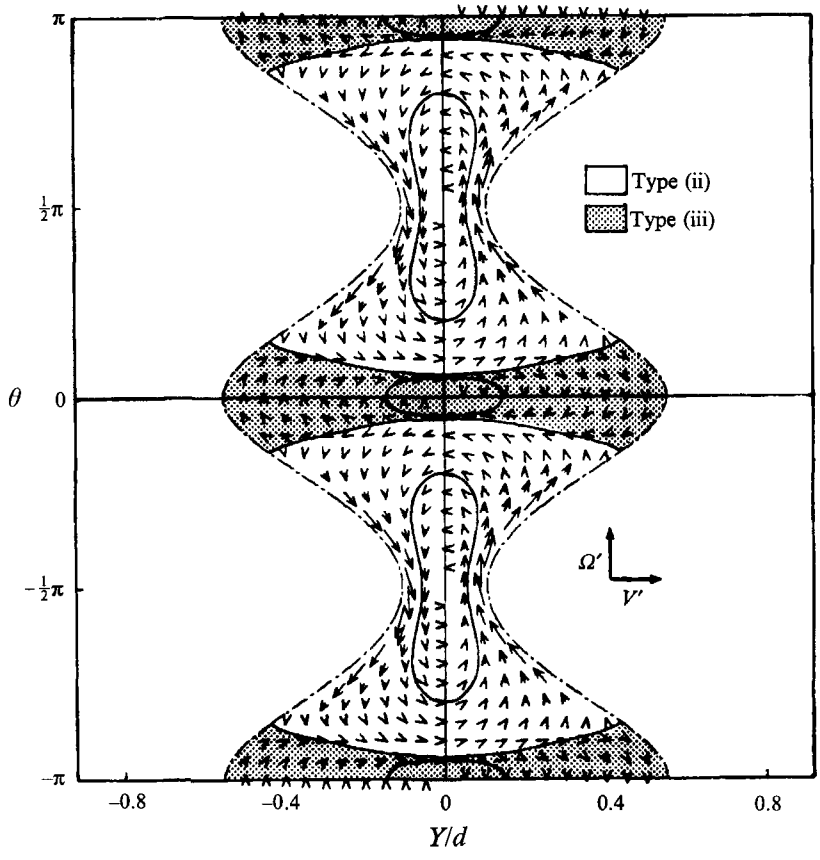

FIGURE 12. Non-dimensional lateral velocity $V' = V/U_{max}$ and angular velocity $\Omega' = \Omega d/U_{max}$ of an elliptic cylinder with $\alpha = 2$ and $\beta = 0.4$ ($a/d = 0.894$, $b/d = 0.447$). ——, representative trajectories of the elliptic cylinder.

threshold β^*, vectors of $(V/U_{max}, \Omega d/U_{max})$ and some representative trajectories of an elliptic cylinder with $\alpha = 2$ and $\beta = 0.4$ are plotted in the $(Y/d, \theta)$-plane in figure 12. The whole region near the Y/d-axis is covered by the type (iii) motion, and the type (i) motion vanishes. It is interesting to note that the origin in the $(Y/d, \theta)$ plane is neutrally stable in figure 12, while it is unstable in figure 9. An explanation as to why the origin in figure 12 is neutrally stable is suggested by lubrication theory and computations for a closely fitting particle in a channel which may be similar for a particle in a tube presented by Secomb & Hsu (1993). At present there is no rigorous explanation for the unstable behaviour at the origin in figure 9.

Typical examples of the time courses of particle velocities, positions, and orientation, and the additional pressure drop for an elliptic cylinder with $\alpha = 2$ and $\beta = 0.4$ are plotted in figure 13. It is seen that each curve in figure 13(*a*) for the type (ii) motion is similar in shape to the corresponding one in figure 10(*b*), although the variation over a period is more significant in figure 13(*a*). In contrast, the behaviours of the variables in the type (iii) motion shown in figure 13(*b*) are qualitatively different from those in figure 10(*c*). In figure 13(*b*), the longitudinal velocity and additional pressure drop have dual peaks within a period, and the particle moves from one side of the channel to the other, changing the direction of rotation at every half period. These features are common to the type (ii) motion (see figure 13*a*). This similarity in the type (ii) and type

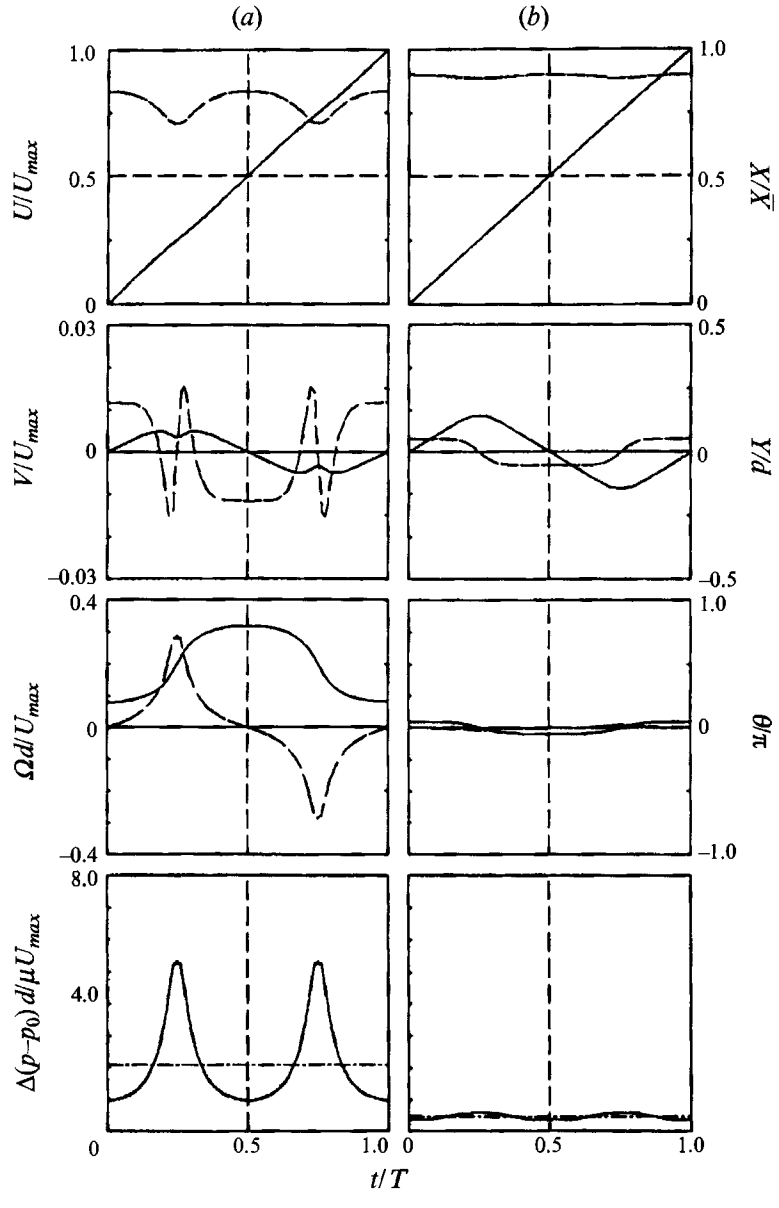

FIGURE 13. Time courses of the positions and orientation of an elliptic cylinder $X/\bar{X}$, $Y/d, \theta$, the velocities U/U_{max}, V/U_{max}, $\Omega d/U_{max}$, and the additional pressure drop $\Delta(p-p_0)\,d/\mu U_{max}$ over a cycle for an elliptic cylinder with $\alpha = 2$ and $\beta = 0.4$. (*a*) Type (ii) motion starting from $(Y/d, \theta) = (0, 0.2\pi)$, (*b*) type (iii) motion starting from $(0, 0.05\pi)$.

(iii) motions in figure 13 may be understood by noting a resemblance in the particle trajectories in figure 12; they are both closed loops, encircling neutrally stable points $(Y/d, \theta) = (0, \pm\frac{1}{2}\pi)$ (type (ii) motion) or $(0, 0)$ (type (iii) motion), where $(0, 0)$ and $(0, \pm\frac{1}{2}\pi)$ represent the configurations of the particle located at the channel centreline with the major or minor axis aligned with the flow, respectively.

The amplitudes of the oscillation in the type (ii) and type (iii) motions increase as the initial configuration is farther apart from the points $(0, 0)$ or $(0, \pm\frac{1}{2}\pi)$ in the $(Y/d, \theta)$-

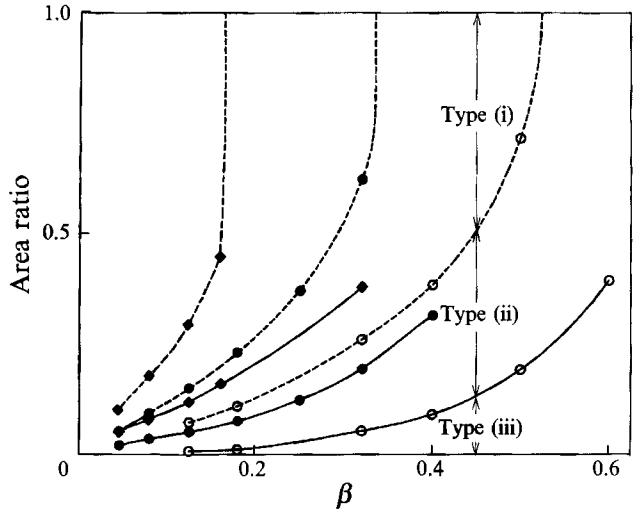

FIGURE 14. Area ratios of the regions of the type (i), type (ii) and type (iii) motions in the $(Y/d, \theta)$-plane, for elliptic cylinders with ○, $\alpha = 1.5$; ●, $\alpha = 2$; and ◆, $\alpha = 3$. The solid curves represent the area of the type (iii) motion with respect to the physically possible configurations in the $(Y/d, \theta)$-plane (see figures 9 and 12), the differences between the solid curves and the corresponding dashed curves represent the area ratios of the type (ii) motion, and the remaining areas (up to the area ratio = 1) correspond to the area ratios of the type (i) motion.

plane. For example, an elliptic cylinder starting near the points $(0, 0)$ or $(0, \pm\frac{1}{2}\pi)$ will stay around the initial configurations, but a particle starting near a channel wall will approach the other wall in half a period. It is interesting to note that, in general, in the type (ii) motion the variation of the orientation within a period is more pronounced than that of the lateral position, while in the type (iii) motion the converse is true.

3.3. *Probability of each type of motion*

A comparison between figures 9 and 12 suggests that an increase in β results in a decrease in the area of the type (i) motion in the $(Y/d, \theta)$-plane, and an increase in the areas of the type (ii) and type (iii) motions. Figure 14 gives the area of each type of motion with respect to the physically possible configurations in the $(Y/d, \theta)$-plane, as a function of β for various axis ratios. As the size ratio β increases, the area ratio of the type (i) motion decreases until it vanishes at $\beta = \beta^*$. The area ratios of the type (ii) and type (iii) motions, on the contrary, increase monotonically with increasing β up to β^*. Since an alternative plot of the area ratios as a function of a/d makes the curves closer to each other, it is suggested that the major axis length rather than β is a dominant determinant of the type of particle motion.

Our study indicates that no particular positions or orientations of an elliptic cylinder in a channel are intrinsically favoured. If the lateral position and orientation of the elliptic cylinder are initially distributed randomly, the area ratios shown in figure 14 may represent the probability of the corresponding type of motion being observed. Figure 14 suggests that for cylinders with a major axis smaller than 50% the channel width, almost all particles exhibit type (i) motion, while for cylinders with a major axis larger than 70–90% the channel width, they execute the type (ii) or type (iii) motion, and none of them undergoes the type (i) motion.

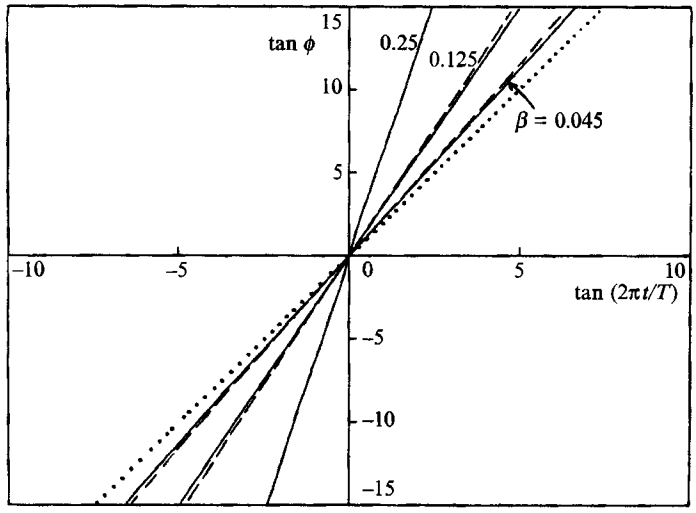

FIGURE 15. Tan ϕ *vs.* tan $(2\pi t/T)$ in the type (i) motion for elliptic cylinders in a channel flow, with $\alpha = 2$ and various β. The lateral positions of the elliptic cylinders at $\phi = 0$ are ——, $Y^{\dagger}/d = 0.15$; – – –, $Y^{\dagger}/d = 0.3$. · · · ·, equation (11) with $r_e = 2$, for comparison.

3.4. *Comparison with the motion of an elliptic cylinder in unbounded flows*

The following equations in the notation given by Jeffery (1922) describe the rotary motion of an elliptic cylinder in an unbounded shear flow:

$$\tan\phi = r_e \tan(2\pi t/T), \tag{11}$$

and

$$T = \frac{2\pi}{\gamma}(r_e + r_e^{-1}), \tag{12}$$

where r_e represents the axis ratio equal to $\alpha(= a/b)$, T denotes the period of motion, γ represents the rate of shear, and ϕ is the angle between the minor axis and the flow direction, which is equal to $(\frac{1}{2}\pi - \theta)$ in the present notation (see figure 1).

For an elliptic cylinder in a channel flow, the time course of the orientation variation during a period shown in figure 10(*a*) suggests a similarity of the type (i) motion to the tumbling motion of Jeffery's solution. To compare our result of the type (i) motion with the tumbling motion in an unbounded shear flow, some results of our computation are replotted in the form of tan ϕ *vs.* tan $(2\pi t/T)$ in figure 15, corresponding to equation (11). It is obvious that tan ϕ is almost linearly proportional to tan $(2\pi t/T)$, and this relationship approximately holds for even rather large elliptic cylinders compared to the channel width, such as $\beta = 0.25$.

As is seen in figure 15, the slopes of the tan ϕ *vs.* tan $(2\pi t/T)$ curves, or the values of r_e in equation (11), which is called an equivalent axis ratio, are different from the actual axis ratio $\alpha(= a/b)$ in a channel flow. The values of r_e can be also evaluated from equation (12), using the period of motion and the local shear rate of the Poiseuille flow evaluated at the particle centroid. The values of r_e determined from equations (11) and (12) are plotted in figure 16, as a function of the lateral position of the cylinder at $\phi = 0$, $Y^{\dagger}$, for $\alpha = 2$ with several values of β. It is seen that the corresponding two values are close to each other except for larger particles. This suggests that the rotary motion of cylinders in the type (i) motion is well approximated by equations (11) and (12) with an appropriate equivalent axis ratio r_e. The values of r_e are shown to be larger than $\alpha(= 2)$ for all cases investigated, and increase with increasing β for given $Y^{\dagger}$. More

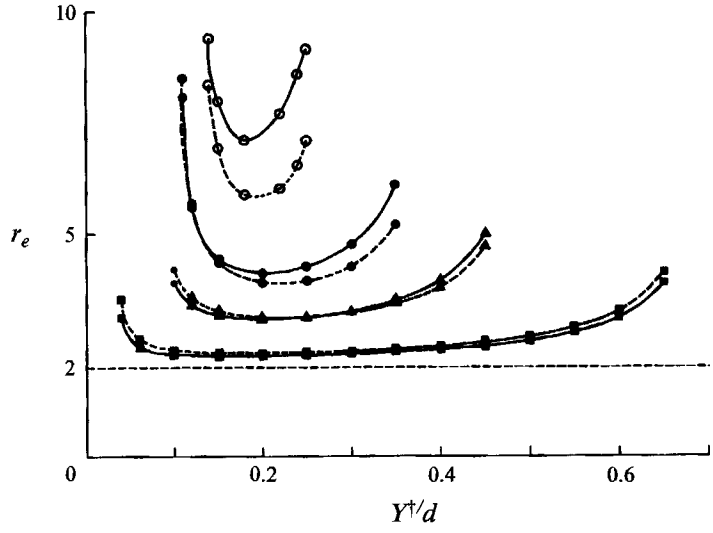

FIGURE 16. The equivalent axis ratios r_e for elliptic cylinders with $\alpha = 2$ and various β, evaluated ——, from equation (11) and – – –, from equation (12) using the computed data for elliptic cylinders motion in a channel flow. The size ratios are ■, $\beta = 0.045$; ▲, $\beta = 0.125$; ●, $\beta = 0.18$; ○, $\beta = 0.25$.

interestingly, an increase of r_e with increasing $Y^\dagger$ for given β indicates that, as a cylinder approaches a wall, the period of rotation increases owing to wall effects.

Stover & Cohen (1990) studied experimentally the motion of rodlike particles freely suspended in a channel flow, and reported that a particle rotates accurately obeying Jeffery's equation, if an equivalent axis ratio is calculated from the observed period of rotation, by use of equation (12). It was also demonstrated that the period of rotation increases up to 50%, as the particle approaches a wall (figure 7 in Stover & Cohen 1990). These observations are in good agreement with our results shown in figures 15 and 16, as long as the particle is small compared to the channel width.

3.5. *Comparison with the motion of a doublet in channel flow*

In the preceding study of the present author (Sugihara-Seki 1992), the motion of a doublet composed of two equal-sized cylinders held in rigid contact in channel flow was analysed. Since the rotary motion of a doublet in unbounded linear flow is known to be equivalent to that of an elliptic cylinder with the axis ratio equal to 1.83 (Raasch 1961; Darabaner, Raasch & Mason 1967), it is interesting to compare their motions in channel flow. Instead of the type (iii) motion, another type of oscillatory motion was obtained for doublets, in which a doublet located near the channel centreline oscillates in orientation with an amplitude less than $\frac{1}{2}\pi$, and moves transversely in an oscillatory manner with its mean at the centreline. It was also demonstrated that the type (i) motion is present as long as it is physically possible, while for elliptic cylinders the type (i) motion is inhibited for $\beta > \beta^*$. These results suggest that a similarity in the motions of a doublet and an elliptic cylinder obtained in unbounded flows does not necessarily hold in channel flows, especially in narrow channel flows. The difference in the particle motion is undoubtedly due to the fact that the hydrodynamic interaction between the particle and the walls is significantly affected by the precise shape of the particle. For the elliptic cylinder shown in figure 7, a pair of the downstream positive and upstream negative pressures appears in the narrower gap region between the particle and the wall, whereas for a doublet at similar configurations, there are two pairs, i.e. one pair

for each cylinder, of such pressure variations. These differences in the pressure distributions result in the rotation of the elliptic cylinder in the clockwise direction (see figures 6*c* and 8*c*) and the rotation of the doublet in the opposite direction at these configurations.

4. Concluding remark

We have presented only two-dimensional numerical solutions for the motion of elliptical cylinders in a channel flow. Since Hu, Joseph & Fortes (1992) showed that many of the three-dimensional observations of the behaviour of particles sedimenting in a channel are coincident with their two-dimensional numerical results, we expect that the present solutions will also predict some features of three-dimensional solutions. However, detailed three-dimensional analyses will be required in cases when the particle approaches a wall to a near contact, because in such cases the difference between two- and three-dimensions, i.e. a line contact *vs.* a point contact may become important.

The author wishes to express her sincere thanks to Professor Richard Skalak of the University of California, San Diego who gave valuable comments, and to Dr Junji Seki for helpful discussions. Also, the author would like to acknowledge the referees for constructive comments and suggestions. This research was supported in part by Grants-in-Aid for Scientific Research from the Ministry of Education, Science and Culture of Japan. The numerical computations were carried out at the Data Processing Center, Kyoto University, and the Computation Center, Osaka University, Japan.

REFERENCES

ARP, P. A. & MASON, S. G. 1977 *J. Colloid Interface Sci.* **61**, 21.

BRETHERTON, F. P. 1962 *J. Fluid Mech.* **14**, 284.

CHEN, T. C. & SKALAK, R. 1970 *Appl. Sci. Res.* **22**, 403.

CHWANG, A. T. 1975 *J. Fluid Mech.* **72**, 17.

COX, R. G., ZIA, I. Y. Z. & MASON, S. G. 1968 *J. Colloid Interface Sci.* **17**, 7.

DĄBROŚ, T. 1985 *J. Fluid Mech.* **156**, 1.

DARABANER, C. L., RAASCH, J. K. & MASON, S. G. 1967 *Can. J. Chem. Engng* **45**, 3.

DVINSKY, A. S. 1983 PhD thesis, Cullen College of Engineering, University of Houston, USA.

DVINSKY, A. S. & POPEL, A. S. 1987 *Comput. Fluids* **15**, 405.

EDWARDES, D. 1892 *Q. J. Maths* **26**, 70.

FAXEN, H. 1946 *Proc. R. Swed. Inst. Engng Res.* **187**, 1.

GANATOS, P., WEINBAUM, W. & PFEFFER, R. 1982 *J. Fluid Mech.* **124**, 27.

HSU, R. 1985 Hydrodynamic interaction of an arbitrary particle with a planar-wall at low Reynolds numbers. PhD thesis, City University of New York, USA.

HSU, R. & GANATOS, P. 1989 *J. Fluid Mech.* **207**, 29.

HU, H. H., JOSEPH, D. D. & FORTES, A. F. 1992 Army High Performance Computing Research Center Preprint 92-035.

JEFFERY, G. B. 1922 *Proc. R. Soc.* A **102**, 161.

KIM, S. & KARRILA, S. J. 1991 *Microhydrodynamics: Principles and Selected Applications.* Butterworth–Heinemann.

OBERBECK, A. 1876 *Crelles J.* **81**, 62.

OLSON, M. D. & TUANN, S. Y. 1978 *Finite Elements in Fluids*, vol. 3, p. 73. Wiley.

RAASCH, J. K. 1961 PhD thesis. Faculty of Mechanical Engineering, Karlsruhe Technical University, Karlsruhe, Germany.

SECOMB, T. W. & HSU, R. 1993 Submitted to *J. Fluid Mech.*
STOVER, C. A. & COHEN, C. 1990 *Rheol. Acta* **29**, 192.
SUGIHARA-SEKI, M. 1992 *Trans. ASME* K: *J. Biomech. Engng* **114**, 547.
SUGIHARA, M. & NIIMI, H. 1984 *ASME J. Appl. Mech.* **51**, 879.
SUGIHARA-SEKI, M., SECOMB, T. W. & SKALAK, R. 1990 *Microvasc. Res.* **40**, 379.
SUGIHARA-SEKI, M. & SKALAK, R. 1988 *Microvasc. Res.* **36**, 64.
SUGIHARA-SEKI, M. & SKALAK, R. 1989 *Biorheology* **26**, 261.
TAKAISI, Y. 1955 *J. Phys. Soc. Japan* **10**, 685.
TAKAISI, Y. 1956 *J. Phys. Soc. Japan* **11**, 1092.
TÖZEREN, H. 1984 *Intl J. Numer. Meth. Fluids* **4**, 159.
WAKIYA, S. 1957 *J. Phys. Soc. Japan* **12**, 1130.
WAKIYA, S. 1959 *Res. Rep Fac. Engng Niigata Univ. Japan* **8**, 31.
WEINBAUM, S., GANATOS, P. & YAN, Z.-Y. 1990 *Ann. Rev. Fluid Mech.* **22**, 275.
YANG, S.-M. & LEAL, G. 1984 *J. Fluid Mech.* **149**, 275.